Available online at www.sciencedirect.com
ScienceDirect
Signal Processing 88 (2008) 1485–1495
SIGNAL PROCESSING
www.elsevier.com/locate/sigpro

Statistical analysis of the LMS adaptive algorithm subjected to a symmetric dead-zone nonlinearity at the adaptive filter output

Márcio Holsbach Costa*, Leandro Ronchini Ximenes, José Carlos Moreira Bermudez

Department of Electrical Engineering, Federal University of Santa Catarina, Florianópolis 88040-900, SC, Brazil

Received 3 September 2007; received in revised form 10 December 2007; accepted 13 December 2007
Available online 23 December 2007

Abstract

This work presents a statistical analysis of the Least Mean Square (LMS) adaptive algorithm subjected to the existence of a symmetric dead-zone nonlinearity at the adaptive filter output. Such configuration can be representative of low-cost active noise control systems where the canceling signal drives a class B power amplifier or a nonlinear actuator. Recursive deterministic equations are derived for the mean coefficient and mean-square error behaviors assuming Gaussian signals and slow adaptation. The steady-state algorithm behavior is determined for given filter parameters and degree of nonlinearity. Monte Carlo simulations and laboratory experiments are presented which corroborate the theoretical results.

Keywords: Adaptive filters; LMS; Dead-zone; Nonlinearity; Active noise control

1. Introduction

Practical adaptive identification and control design techniques usually tend to ignore the presence of nonlinearities in real applications [1,2]. The main reason for that seems to be the difficulty in obtaining theoretical models capable of predicting the performance of the adaptive algorithms under the influence of such nonlinearities.

Static (e.g. dead-zone or saturation) and dynamic (e.g. backlash or hysteresis) nonlinearities present in several physical systems are often neglected for simplicity. They occur in most mechanical, hydraulic, electronic and biological systems [3]. Among the static nonlinearities, the dead-zone has been widely employed to model physical phenomena that present negligible dynamics when compared to the system time constants. These phenomena are characterized by a negligible response to a range of input signal amplitudes [4].

Dead-zones can originate from different causes. Important examples are the dry friction or stiction in electromechanical and hydraulic systems (such as in servomotors and servovalves), the physical imperfections in sensors and actuators [2], or the cut-in voltage in low-cost power amplifiers (crossover effect) [5]. Although dead-zones can be avoided to some extent by careful electronic or mechanical design, sometimes this effort can excessively increase design and manufacturing costs. In some

*Corresponding author. Tel.: +55 48 3721 9506; fax: +55 48 3721 9280.
E-mail addresses: costa@eel.ufsc.br (M.H. Costa), lrximenes@yahoo.com.br (L.R. Ximenes), j.bermudez@ieee.org (J.C.M. Bermudez).

0165-1684/$ - see front matter © 2008 Elsevier B.V. All rights reserved.
doi:10.1016/j.sigpro.2007.12.008

situations, however, the presence of a dead-zone is unavoidable, such as in biological systems [6,7].

Dead-zone nonlinearities have been mostly studied in the robust control literature. It has been recognized that actuator and sensor nonlinearities are among the key factors limiting both the static and dynamic performances of feedback control systems [3]. The most straightforward way to cope with dead-zone nonlinearities is to cancel them by employing their inverse functions. However, this can be done only when the dead-zone nonlinearity is exactly known. In general its parameters are unknown and may vary in time and with operating conditions [8].

Several approaches have been proposed to deal with dead-zone nonlinearities, which include the use of fuzzy logic and neural networks. Unfortunately, such approaches are usually associated with a large computational complexity. In addition, ''industrialists often view these techniques with some apprehension and distrust'' [1]. As a result, linear adaptive control techniques provide an attractive solution whenever minimum satisfactory performance objectives can be guaranteed.

Two important application systems that are affected by dead-zone nonlinearities are active noise control (ANC) and active vibration control (AVC) systems [9–11]. The nonlinearity is introduced by vibrational transducers (generally piezoelectric or loudspeakers) and/or by low-cost power amplifiers. These elements process the adaptive filter output[1] to generate the acoustic or vibrational waves required to interfere destructively with the field caused by the original source of disturbance. Nowadays, such systems are available in many commercial products, especially in avionics and in the vehicle industry. For these systems to be competitive, they should employ inexpensive transducers and amplifiers, especially because most of them are multichannel. Besides economical considerations, energy efficiency is a major concern in power amplifier design, frequently leading to the use of nonlinear class B power amplifiers.

Few works in the literature provide analytical descriptions of the behavior of adaptive filters when affected by nonlinearities. Nevertheless, recent studies have shown that nonlinearities can have a significant impact on the adaptive filter performance [12–15]. Thus, it is of great interest for the designer to have theoretical models capable of predicting the system performance based on approximated bounds of the nonlinear characteristic [16]. The influence of a dead-zone on the RLS adaptive filter behavior has been studied in Ref. [17]. However, to the best knowledge of the authors, there is no available model for predicting the performance of the widespread Least Mean Square (LMS) adaptive filter family with dead-zone output nonlinearity [18–20].

This work studies the effects of a symmetric secondary-path dead-zone nonlinearity on the stochastic performance of LMS-based adaptive systems. The analysis presented here considers a memoryless nonlinear secondary-path. The analysis can be readily extended to incorporate a linear filtering operation to the secondary-path in the light of Ref. [13].

The paper is organized as follows. Section 2 presents the analyzed topology and the dead-zone analytical description and modeling. Section 3 provides an analysis of the mean weight behavior of the LMS adaptive filter subjected to an output dead-zone nonlinearity for Gaussian input signals. Section 4 presents an expression for the mean-square error (MSE) under slow adaptation conditions. Section 5 presents a recursive equation for the second-order moments required for the evaluation of the MSE. Section 6 presents steady-state results. Sections 7 and 8 present, respectively, simulation and experimental results that corroborate the main theoretical properties derived. Finally, Section 9 presents the main conclusions.

2. Dead-zone modeling

The studied system is presented in Fig. 1. Assuming an ANC application, $d(n)$ is the signal to be canceled, $y(n)$ is the output of the adaptive canceler, $e(n)$ is the error signal, $z(n)$ is the measurement noise, which is zero-mean with variance $r_z = E\{z^2(n)\}$, independent and identically distributed and uncorrelated with the input signal. The input signal $x(n)$ is assumed stationary, Gaussian, with zero-mean and variance $r_x = E\{x^2(n)\}$. The input and weight vectors are defined as $\mathbf{x}(n) = [x(n),\ x(n-1),\ \ldots,\ x(n-N+1)]^{\mathrm{T}}$ and $\mathbf{w}(n) = [w_0(n),\ w_1(n),\ \ldots,\ w_{N-1}(n)]^{\mathrm{T}}$, respectively, both with dimension N. The vector $\mathbf{w^o} = [w_0^{\mathrm{o}}, w_1^{\mathrm{o}}, \ldots, w_{N-1}^{\mathrm{o}}]^{\mathrm{T}}$ is the impulse response of the unknown system. The dead-zone nonlinear characteristic is represented by the $g_{\mathrm{DZ}}(\cdot)$ block. Its input–output relation is

[1]They incorporate what is frequently described as the secondary-path [9].

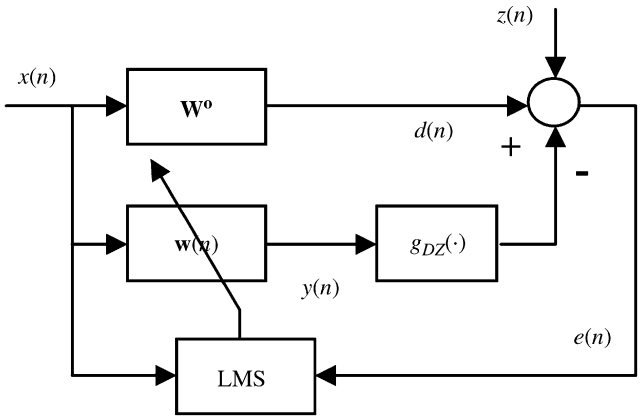

Fig. 1. Adaptive system.

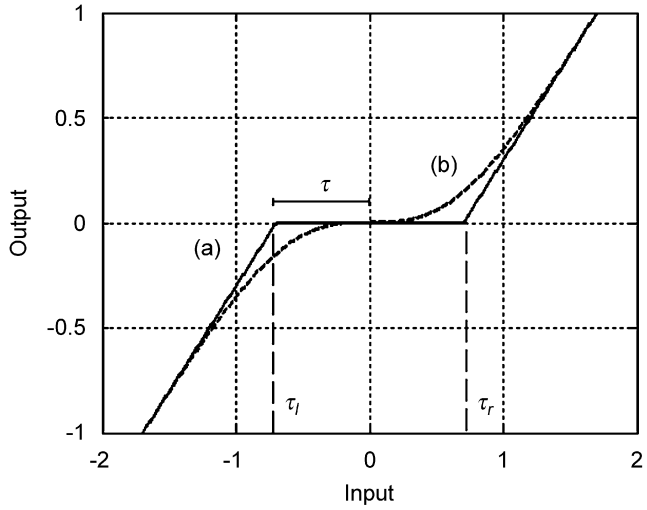

Fig. 2. Dead-zone nonlinearity: (a) hard and (b) soft approximation by the error function.

given by [3]

$$g_{\mathrm{DZ}}[y(n)] = \begin{cases} m_{\mathrm{r}}[y(n) - \tau_{\mathrm{r}}] & \text{for } y(n) \geqslant \tau_{\mathrm{r}} \\ 0 & \text{for } \tau_{\mathrm{l}} < x(n) < \tau_{\mathrm{r}}, \\ m_{\mathrm{l}}[y(n) - \tau_{\mathrm{l}}] & \text{for } y(n) \leqslant \tau_{\mathrm{l}} \end{cases} \quad (1)$$

and depicted in Fig. 2, where m_{r} and m_{l} are the angular coefficients of the right and left portions of the nonlinearity, respectively. τ_{r} and τ_{l} are the right and left limits of the dead-zone.

2.1. Dead-zone modeling

To facilitate the development of analytical models, it is convenient to approximate the piecewise nonlinearity given by Eq. (1) by a continuous and more mathematically tractable function (in light of the Gaussianity of the input signals). The dead-zone nonlinearity can be decomposed as [1]

$$g_{\mathrm{DZ}}[y(n)] = \begin{cases} m_{\mathrm{r}} y(n) - g_{\mathrm{SAT}}[y(n)] & \text{for } y(n) < 0 \\ m_{\mathrm{l}} y(n) - g_{\mathrm{SAT}}[y(n)] & \text{for } y(n) > 0 \end{cases} \quad (2)$$

where $g_{\mathrm{SAT}}(\cdot)$ is the saturation nonlinearity given by

$$g_{\mathrm{SAT}}[y(n)] = \begin{cases} m_{\mathrm{r}} y(n) & \text{for } 0 \leqslant y(n) < \tau_{\mathrm{r}} \\ m_{\mathrm{l}} y(n) & \text{for } \tau_{\mathrm{l}} \leqslant y(n) < 0 \\ m_{\mathrm{r}} \tau_{\mathrm{r}} & \text{for } y(n) > \tau_{\mathrm{r}} \\ m_{\mathrm{l}} \tau_{\mathrm{l}} & \text{for } y(n) < \tau_{\mathrm{l}} \end{cases}. \quad (3)$$

In general, neither the break-points $(\tau_{\mathrm{l}}, \tau_{\mathrm{r}})$ are symmetrical about zero nor the slopes $(m_{\mathrm{r}}, m_{\mathrm{l}})$ are equal [3]. However, nonlinearities encountered in many applications (including biomedical and mechanical systems) can often be approximated with success by the symmetry conditions assuming $m_{\mathrm{r}} = m_{\mathrm{l}}$ and $\tau_{\mathrm{r}} = -\tau_{\mathrm{l}}$. This approximation is especially good in the case of class B amplifiers, where the dead-zone nonlinearity is due to a complementary pair of transistors.

The error function has been successfully used as an approximation of a saturation-type nonlinearity in deriving analytical models for the LMS family [12–15]. Assuming symmetry and unit gain $(m_{\mathrm{r}} = m_{\mathrm{l}} = 1 \text{ and } \tau_{\mathrm{r}} = -\tau_{\mathrm{l}} = \tau)$, the dead-zone nonlinearity can be approximated by

$$\hat{g}_{\mathrm{DZ}}[y(n)] = y(n) - g[y(n)] = y(n) - \int_0^{y(n)} \mathrm{e}^{-z^2/2\sigma^2}\, \mathrm{d}z, \quad (4)$$

where $y(n)$ is the input to the dead-zone nonlinearity and $g(\cdot)$ is the error function. The σ parameter in $g(\cdot)$ is given by

$$\sigma^2 = \frac{2}{\pi}\tau^2, \quad (5)$$

so that Eq. (4) approximates the nonlinearity in Fig. 2.

3. Mean weight behavior

The LMS update weight equation is defined as [19]

$$\mathbf{w}(n+1) = \mathbf{w}(n) + \mu e(n)\mathbf{x}(n). \quad (6)$$

From Fig. 1, the estimation error is

$$e(n) = \mathbf{w}^{\mathrm{oT}}\mathbf{x}(n) + z(n) - g_{\mathrm{DZ}}[\mathbf{w}^{\mathrm{T}}(n)\mathbf{x}(n)]. \quad (7)$$

Substituting Eq. (4) for g_{DZ} [.] in Eq. (7) we obtain

$$e(n) = \mathbf{w}^{\mathrm{oT}}\mathbf{x}(n) + z(n) - \mathbf{w}^{\mathrm{T}}(n)\mathbf{x}(n) + g[\mathbf{w}^{\mathrm{T}}(n)\mathbf{x}(n)]. \quad (8)$$

Using Eq. (8) in Eq. (6) and taking expectations conditioned on the weight vector $\mathbf{w}(n)$ it comes to

$$E\{\mathbf{w}(n+1)|\mathbf{w}(n)\} = E\{[\mathbf{I}-\mu\mathbf{x}(n)\mathbf{x}^{\mathrm{T}}(n)]\mathbf{w}(n)|\mathbf{w}(n)\} + \mu E\{g[\mathbf{w}^{\mathrm{T}}(n)\mathbf{x}(n)]\mathbf{x}(n)|\mathbf{w}(n)\} + \mu\mathbf{R}\mathbf{w}^{\mathbf{o}}, \quad (9)$$

where $\mathbf{R} = E\{\mathbf{x}(n)\mathbf{x}^{\mathrm{T}}(n)\}$ is the input vector autocorrelation matrix. Neglecting the statistical dependence between the coefficient and input signal vectors [21],[2] the first term in Eq. (9) becomes

$$E\{[\mathbf{I}-\mu\mathbf{x}(n)\mathbf{x}^{\mathrm{T}}(n)]\mathbf{w}(n)|\mathbf{w}(n)\} \cong [\mathbf{I}-\mu\mathbf{R}]\mathbf{w}(n). \quad (10)$$

The second expectation in Eq. (9) can be obtained as in Ref. [14], Eq. (20), resulting in

$$E\{g[\mathbf{w}^{\mathrm{T}}(n)\mathbf{x}(n)]\mathbf{x}(n)|\mathbf{w}(n)\} \approx \left(\frac{1}{\sigma^2}\mathbf{w}^{\mathrm{T}}(n)\mathbf{R}\mathbf{w}(n)+1\right)^{-1/2}\mathbf{R}\mathbf{w}(n). \quad (11)$$

Using Eqs. (10) and (11) in Eq. (9) and taking the expectation over $\mathbf{w}(n)$, $E\{\mathbf{w}(n+1)\}$ can be approximated by

$$E\{\mathbf{w}(n+1)\} = \left[\mathbf{I}-\mu\mathbf{R}+\mu\left(\frac{1}{\sigma^2}\mathrm{tr}\{\mathbf{R}\mathbf{K}(n)\}+1\right)^{-1/2}\mathbf{R}\right] \times E\{\mathbf{w}(n)\} + \mu\mathbf{R}\mathbf{w}^{\mathbf{o}}. \quad (12)$$

In deriving the expected value of Eq. (11) to obtain Eq. (12) we have approximated $\mathbf{w}^{\mathrm{T}}(n)\mathbf{R}\mathbf{w}(n)$ by its expected value $\mathrm{tr}\{\mathbf{R}\mathbf{K}(n)\}$ where $\mathbf{K}(n) = E\{\mathbf{w}(n)\mathbf{w}^{\mathrm{T}}(n)\}$ is the weight vector correlation matrix. This approximation, required for mathematical tractability, neglects the fluctuations of the weighted norm of $\mathbf{w}(n)$, ($||\mathbf{w}(n)||_{\mathbf{R}}$, [22]), as compared to its mean value. It becomes more accurate as the step size decreases and the order of the adaptive filter increases. Eq. (12) is a deterministic recursive model of the mean weight behavior. In the particular case of white input signal Eq. (12) reduces to

$$E\{\mathbf{w}(n+1)\} = \left[1-\mu r_x+\mu r_x\left(\frac{r_x}{\sigma^2}T_k(n)+1\right)^{-1/2}\right] \times E\{\mathbf{w}(n)\} + \mu r_x\mathbf{w}^{\mathbf{o}}, \quad (13)$$

where $T_k(n) = \mathrm{tr}\{\mathbf{K}(n)\}$.

Note that even after all the approximations, the mean weight model still keeps effects of the second-order moments of $\mathbf{w}(n)$, which are imposed by the nonlinearity.

[2]This approximation corresponds to the well-known independence assumption and is more valid for slow adaptation.

4. Mean-square error

Squaring Eq. (8) and taking the expected value of the result, conditioned on $\mathbf{w}(n)$, leads to

$$E\{e^2(n)|\mathbf{w}(n)\} = \mathbf{w}^{\mathbf{o}\mathrm{T}}\mathbf{R}\mathbf{w}^{\mathbf{o}} + E\{z^2(n)\} + 2\mathbf{w}^{\mathbf{o}\mathrm{T}}E\{g[\mathbf{w}^{\mathrm{T}}(n)\mathbf{x}(n)]\mathbf{x}(n)|\mathbf{w}(n)\} - 2\mathbf{w}^{\mathrm{T}}(n)E\{g[\mathbf{w}^{\mathrm{T}}(n)\mathbf{x}(n)]\mathbf{x}(n)|\mathbf{w}(n)\} + E\{g^2[\mathbf{w}^{\mathrm{T}}(n)\mathbf{x}(n)]|\mathbf{w}(n)\} + \mathbf{w}^{\mathrm{T}}(n)\mathbf{R}\mathbf{w}(n) - 2\mathbf{w}^{\mathbf{o}\mathrm{T}}\mathbf{R}\mathbf{w}(n). \quad (14)$$

Using the same approximations and assumptions used in evaluating Eq. (11), the last expectation in Eq. (14) results in [14]

$$E\{g^2[\mathbf{w}^{\mathrm{T}}(n)\mathbf{x}(n)]|\mathbf{w}(n)\} \approx \sigma^2 \arcsin\left(\frac{\mathbf{w}^{\mathrm{T}}(n)\mathbf{R}\mathbf{w}(n)}{\mathbf{w}^{\mathrm{T}}(n)\mathbf{R}\mathbf{w}(n)+\sigma^2}\right). \quad (15)$$

Using Eqs. (11) and (15) in Eq. (14) we obtain

$$E\{e^2(n)\} = \mathbf{w}^{\mathbf{o}\mathrm{T}}\mathbf{R}\mathbf{w}^{\mathbf{o}} + r_z + \mathrm{tr}\{\mathbf{R}\mathbf{K}(n)\} - 2\mathbf{w}^{\mathbf{o}\mathrm{T}}\mathbf{R}E\{\mathbf{w}(n)\} + 2\left(\frac{1}{\sigma^2}\mathrm{tr}\{\mathbf{R}\mathbf{K}(n)\}+1\right)^{-1/2} \times [\mathbf{w}^{\mathbf{o}\mathrm{T}}\mathbf{R}E\{\mathbf{w}(n)\} - \mathrm{tr}\{\mathbf{R}\mathbf{K}(n)\}] + \sigma^2 \arcsin\left(\frac{\mathrm{tr}\{\mathbf{R}\mathbf{K}(n)\}}{\mathrm{tr}\{\mathbf{R}\mathbf{K}(n)\}+\sigma^2}\right). \quad (16)$$

Eq. (16) is a theoretical description of the mean-square error evolution with time. For the white input case Eq. (16) simplifies to

$$E\{e^2(n)\} = r_x\mathbf{w}^{\mathbf{o}\mathrm{T}}\mathbf{w}^{\mathbf{o}} + r_z + r_xT_k(n) - 2r_x\mathbf{w}^{\mathbf{o}\mathrm{T}}E\{\mathbf{w}(n)\} + 2r_x\left(\frac{r_x}{\sigma^2}T_k(n)+1\right)^{-1/2} \times \left[\mathbf{w}^{\mathbf{o}\mathrm{T}}E\{\mathbf{w}(n)\} - T_k(n)\right] + \sigma^2 \arcsin\left(\frac{r_xT_k(n)}{r_xT_k(n)+\sigma^2}\right). \quad (17)$$

Since both Eqs. (12) and (16) require the determination of $\mathbf{K}(n) = E\{\mathbf{w}(n)\mathbf{w}^{\mathrm{T}}(n)\}$, this expected value is evaluated in the next section.

5. Second-order moments

Using Eq. (8) in Eq. (6), multiplying the resulting expression by its transposed and taking the

expectation leads to

$$
\begin{aligned}
&E\{\mathbf{w}(n+1)\mathbf{w}^{\mathrm{T}}(n+1)\}\\
&\quad = E\{\mathbf{w}(n)\mathbf{w}^{\mathrm{T}}(n)\} + \mu^2 E\{z^2(n)\}E\{\mathbf{x}(n)\mathbf{x}^{\mathrm{T}}(n)\}\\
&\qquad - \mu E\{\mathbf{w}(n)\mathbf{w}^{\mathrm{T}}(n)\}E\{\mathbf{x}(n)\mathbf{x}^{\mathrm{T}}(n)\}\\
&\qquad - \mu E\{\mathbf{x}(n)\mathbf{x}^{\mathrm{T}}(n)\}E\{\mathbf{w}(n)\mathbf{w}^{\mathrm{T}}(n)\}\\
&\qquad + \mu E\{\mathbf{w}(n)\}\mathbf{w}^{\mathbf{o}\mathrm{T}}E\{\mathbf{x}(n)\mathbf{x}^{\mathrm{T}}(n)\}\\
&\qquad + \mu E\{\mathbf{x}(n)\mathbf{x}^{\mathrm{T}}(n)\}\mathbf{w}^{\mathbf{o}}E\{\mathbf{w}^{\mathrm{T}}(n)\}\\
&\qquad + \mu E\{\mathbf{w}(n)g[\mathbf{w}^{\mathrm{T}}(n)\mathbf{x}(n)]\mathbf{x}^{\mathrm{T}}(n)\}\\
&\qquad + \mu E\{g[\mathbf{w}^{\mathrm{T}}(n)\mathbf{x}(n)]\mathbf{x}(n)\mathbf{w}^{\mathrm{T}}(n)\}\\
&\qquad + \mu^2 E\{\mathbf{x}(n)\mathbf{x}^{\mathrm{T}}(n)\mathbf{w}(n)\mathbf{w}^{\mathrm{T}}(n)\mathbf{x}(n)\mathbf{x}^{\mathrm{T}}(n)\}\\
&\qquad + \mu^2 E\{\mathbf{x}(n)\mathbf{x}^{\mathrm{T}}(n)\mathbf{w}^{\mathbf{o}}\mathbf{w}^{\mathbf{o}\mathrm{T}}\mathbf{x}(n)\mathbf{x}^{\mathrm{T}}(n)\}\\
&\qquad - \mu^2 E\{\mathbf{x}(n)\mathbf{x}^{\mathrm{T}}(n)\mathbf{w}^{\mathbf{o}}\mathbf{w}^{\mathrm{T}}(n)\mathbf{x}(n)\mathbf{x}^{\mathrm{T}}(n)\}\\
&\qquad - \mu^2 E\{\mathbf{x}(n)\mathbf{x}^{\mathrm{T}}(n)\mathbf{w}(n)\mathbf{w}^{\mathbf{o}T}\mathbf{x}(n)\mathbf{x}^{T}(n)\}\\
&\qquad + 2\mu^2 E\{g[\mathbf{w}^{\mathrm{T}}(n)\mathbf{x}(n)]\mathbf{w}^{\mathbf{o}\mathrm{T}}\mathbf{x}(n)\mathbf{x}(n)\mathbf{x}^{\mathrm{T}}(n)\}\\
&\qquad - 2\mu^2 E\{g[\mathbf{w}^{\mathrm{T}}(n)\mathbf{x}(n)]\mathbf{w}^{\mathrm{T}}(n)\mathbf{x}(n)\mathbf{x}(n)\mathbf{x}^{\mathrm{T}}(n)\}\\
&\qquad + \mu^2 E\{g^2[\mathbf{w}^{\mathrm{T}}(n)\mathbf{x}(n)]\mathbf{x}(n)\mathbf{x}^{\mathrm{T}}(n)\}. \qquad (18)
\end{aligned}
$$

The solutions to the expectations in Eq. (18) can be obtained in the same way as in Ref. [14], and using the same assumptions and approximations used for Eqs. (12) and (16), resulting in

$$
\begin{aligned}
\mathbf{K}(n+1) &= \mathbf{K}(n) - \mu\mathbf{K}(n)\mathbf{R} - \mu\mathbf{R}\mathbf{K}(n)\\
&\quad + \mu\mathbf{R}\mathbf{w}^{\mathbf{o}}E\{\mathbf{w}^{\mathrm{T}}(n)\} + \mu E\{\mathbf{w}(n)\}\mathbf{w}^{\mathbf{o}\mathrm{T}}\mathbf{R}\\
&\quad + \mu^2 r_z\mathbf{R} + 2\mu^2\mathbf{R}\mathbf{w}^{\mathbf{o}}\mathbf{w}^{\mathbf{o}\mathrm{T}}\mathbf{R} + \mu^2\mathbf{w}^{\mathbf{o}\mathrm{T}}\mathbf{R}\mathbf{w}^{\mathbf{o}}\mathbf{R}\\
&\quad + 2\mu^2\mathbf{R}\mathbf{K}(n)\mathbf{R} + \mu^2\,\mathrm{tr}\{\mathbf{R}\mathbf{K}(n)\}\mathbf{R}\\
&\quad - 2\mu^2\mathbf{R}\mathbf{w}^{\mathbf{o}}E\{\mathbf{w}^{\mathrm{T}}(n)\}\mathbf{R} - 2\mu^2\mathbf{R}E\{\mathbf{w}(n)\}\mathbf{w}^{\mathbf{o}\mathrm{T}}\mathbf{R}\\
&\quad - 2\mu^2\mathbf{w}^{\mathbf{o}\mathrm{T}}\mathbf{R}E\{\mathbf{w}(n)\}R\\
&\quad + \frac{2\mu^2}{\sigma^2}\left(\frac{1}{\sigma^2}\,\mathrm{tr}\{\mathbf{R}\mathbf{K}(n)\} + 1\right)^{-3/2}\\
&\quad \times [\mathbf{w}^{\mathbf{o}\mathrm{T}}\mathbf{R}E\{\mathbf{w}(n)\} - \mathrm{tr}\{\mathbf{R}\mathbf{K}(n)\}]\mathbf{R}\mathbf{K}(n)\mathbf{R}\\
&\quad + 2\mu^2\left(\frac{1}{\sigma^2}\,\mathrm{tr}\{\mathbf{R}\mathbf{K}(n)\} + 1\right)^{-1}\\
&\quad \times \left(\frac{2}{\sigma^2}\,\mathrm{tr}\{\mathbf{R}\mathbf{K}(n)\} + 1\right)^{-1/2}\\
&\quad \times \mathbf{R}\mathbf{K}(n)\mathbf{R} + \mu\left(\frac{1}{\sigma^2}\,\mathrm{tr}\{\mathbf{R}\mathbf{K}(n)\} + 1\right)^{-1/2}\\
&\quad \times [\mathbf{K}(n)\mathbf{R} + \mathbf{R}\mathbf{K}(n)]\\
&\quad + 2\mu^2\left(\frac{1}{\sigma^2}\,\mathrm{tr}\{\mathbf{R}\mathbf{K}(n)\} + 1\right)^{-1/2}\\
&\quad \times [\mathbf{w}^{\mathbf{o}\mathrm{T}}\mathbf{R}E\{\mathbf{w}(n)\}\mathbf{R} + \mathbf{R}E\{\mathbf{w}(n)\}\mathbf{w}^{\mathbf{o}\mathrm{T}}\mathbf{R}\\
&\quad + \mathbf{R}\mathbf{w}^{\mathbf{o}}E\{\mathbf{w}^{\mathrm{T}}(n)\}\mathbf{R} - 2\mathbf{R}\mathbf{K}(n)\mathbf{R}\\
&\quad - \mathrm{tr}\{\mathbf{R}\mathbf{K}(n)\}\mathbf{R}]\\
&\quad + \mu^2\sigma^2\,\arcsin\left(\frac{\mathrm{tr}\{\mathbf{R}\mathbf{K}(n)\}}{\mathrm{tr}\{\mathbf{R}\mathbf{K}(n)\} + \sigma^2}\right)\mathbf{R}. \qquad (19)
\end{aligned}
$$

Eq. (19) is a recursion for predicting the time evolution of the second-order moments. For the white input signal case, it reduces to

$$
\begin{aligned}
T_k(n+1) &= [1 - 2\mu r_x + \mu^2(N+2)r_x^2]\\
&\quad \times T_k(n) + \mu^2(N+2)\\
&\quad \times r_x^2\mathbf{w}^{\mathbf{o}\mathrm{T}}\mathbf{w}^{\mathbf{o}} + \mu^2 N r_x r_z\\
&\quad + 2\mu r_x[1 - \mu(N+2)r_x]\mathbf{w}^{\mathbf{o}\mathrm{T}}E\{\mathbf{w}(n)\}\\
&\quad + 2\mu^2 r_x^2\left(\frac{2r_x}{\sigma^2}T_k(n) + 1\right)^{-1/2}\\
&\quad \times \left(\frac{r_x}{\sigma^2}T_k(n) + 1\right)^{-1}T_k(n)\\
&\quad + 2\mu r_x\left(\frac{r_x}{\sigma^2}T_k(n) + 1\right)^{-1/2}\\
&\quad \times [\mu(N+2)r_x\mathbf{w}^{\mathbf{o}\mathrm{T}}E\{\mathbf{w}(n)\}\\
&\quad + (1 - \mu(N+2)r_x)T_k(n)]\\
&\quad + \frac{2\mu^2 r_x^3}{\sigma^2}\left(\frac{r_x}{\sigma^2}T_k(n) + 1\right)^{-3/2}\\
&\quad \times [\mathbf{w}^{\mathbf{o}\mathrm{T}}E\{\mathbf{w}(n)\} - T_k(n)]T_k(n)\\
&\quad + \mu^2 r_x N\sigma^2\,\arcsin\left(\frac{r_x T_k(n)}{r_x T_k(n) + \sigma^2}\right). \qquad (20)
\end{aligned}
$$

The complete analytical model for the behavior of the LMS algorithm subjected to the dead-zone nonlinearity in the secondary-path is composed by Eqs. (12), (16) and (19).

The developed analysis makes use of the slow adaptation assumption. Thus, as a further simplification, approximated results can be obtained by disregarding the terms multiplied by μ^2, except for the driving term ($\mu^2 r_z\mathbf{R}$). The result of such procedure is a very fast computational model for small step sizes.

6. Steady-state behavior

This section describes the steady-state behavior of the mean weight and mean-square error using the derived theoretical models.

6.1. Steady-state mean weight behavior

Assuming convergence of Eq. (12) ($\lim_{n\to\infty} E\{\mathbf{w}(n)\} \cong \lim_{n\to\infty} E\{\mathbf{w}(n+1)\}$) and neglecting the fluctuations of $\mathbf{w}(n)$ about its mean value (slow adaptation assumption) leads to

$$\lim_{n\to\infty} E\{\mathbf{w}(n)\} \cong \left[1-\left(\frac{1}{\sigma^2}\lim_{n\to\infty} E\{\mathbf{w}^{\mathrm{T}}(n)\}\mathbf{R}E\{\mathbf{w}(n)\}+1\right)^{-1/2}\right]^{-1}\mathbf{w}^{\mathbf{o}}. \tag{21}$$

Observing Eq. (21) it can be verified that

$$\lim_{n\to\infty} E\{\mathbf{w}(n)\} = q\mathbf{w}^{\mathbf{o}}, \tag{22}$$

where $q \in \mathbb{R}^+$ is a scalar. Using Eq. (22) in Eq. (21) leads to the following relation:

$$\eta^2 q^4 - 2\eta^2 q^3 + \eta^2 q^2 - 2q + 1 = 0, \tag{23}$$

where

$$\eta^2 = \frac{\pi}{2\tau^2}\mathbf{w}^{\mathbf{o}\mathrm{T}}\mathbf{R}\mathbf{w}^{\mathbf{o}}. \tag{24}$$

The expression $1/\eta^2$ is called the system degree of nonlinearity. Differently from the degree of nonlinearity defined in Ref. [14], here the system linearity increases as $\eta^2 \to \infty$. The multiplicative factor q is completely determined by the degree of nonlinearity. It can be easily verified that $q \to 1$ as $\eta^2 \to \infty$, which corresponds to the Wiener solution to the linear case.

Relation (23) is a biquadratic equation ([23], p. 83). The sufficient condition for a root of Eq. (23) to be a solution of Eq. (22) is that it must be positive and real for all $\eta^2 \in [0, \infty)$ (see Eq. (21)). Numerical analysis of Eq. (23) demonstrates the existence of only one solution. Its closed form can be easily obtained using the symbolic calculation tools available in data manipulation softwares. Fig. 3 presents q as a function of η^2.

From this analysis it can be concluded that the steady-state mean weight vector is a scaled version of the Wiener solution to the linear case.

6.2. Steady-state mean-square error behavior

An approximation to the steady-state excess mean-square error (EMSE) can be obtained assuming mean convergence of the coefficients ($\lim_{n\to\infty} E\{\mathbf{w}(n)\} \cong \lim_{n\to\infty} E\{\mathbf{w}(n+1)\}$) and neglecting the fluctuations of $\mathbf{w}(n)$ about its mean value (slow adaptation assumption) in Eq. (16). As a result,

$$\mathrm{EMSE} = \lim_{n\to\infty} E\{e^2(n)\} - r_z \cong v\mathbf{w}^{\mathbf{o}\mathrm{T}}\mathbf{R}\mathbf{w}^{\mathbf{o}}, \tag{25}$$

where

$$v = 1 - 2q + q^2 + \frac{2q(1-q)}{\sqrt{\eta^2 q^2 + 1}} + \frac{1}{\eta^2}\arcsin\left(\frac{\eta^2 q^2}{\eta^2 q^2 + 1}\right). \tag{26}$$

The steady-state mean-square error is also a function of the degree of nonlinearity as expected. Fig. 4 presents the relation between the parameter v and the degree of nonlinearity.

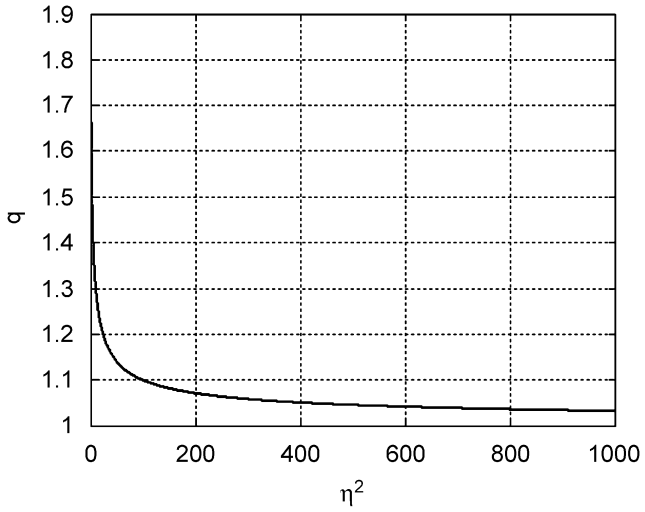

Fig. 3. Steady-state coefficient multiplicative factor (q) as a function of η^2.

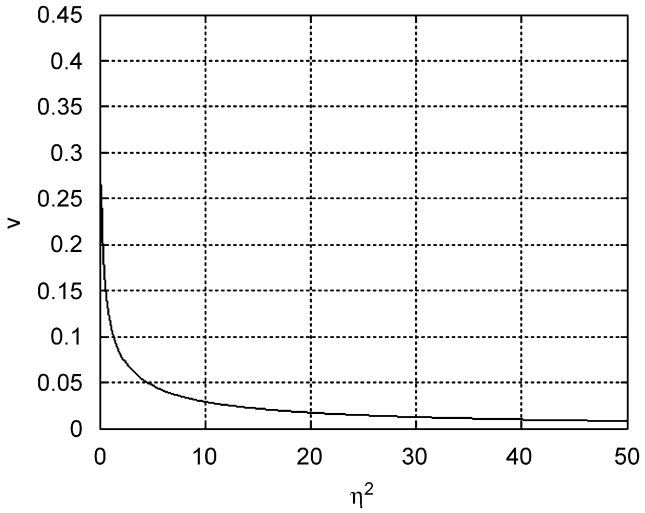

Fig. 4. Steady-state MSE multiplicative factor (v) as a function of η^2.

7. Simulations

In this section, Monte Carlo simulations are presented in order to verify the assumptions and the accuracy of the derived theoretical models. Three examples present comparisons between simulation results and the theoretical predictions using the analytical models described by Eqs. (12), (16) and (19). Unless stated otherwise, all simulated examples share the following common characteristics: the input signal is zero-mean Gaussian with unit power ($r_x = 1$). The additive measurement noise is zero-mean, independent and identically distributed, Gaussian and uncorrelated with the input signal. Initialization was at $\mathbf{w}(0) = [0\,0\,0\,\ldots\,0]^{\mathrm{T}}$. The simulated EMSE was obtained by averaging 500 runs, resulting in a 99% confidence interval for a variation of ± 0.73 dB ([24], p. 314). The used step-size corresponds to $\mu_{\max}/100$, where $\mu_{\max}$ is the maximum step-size[3] that allows adaptive filter convergence for the linear case (the nonlinear system maintains the same stability limit). The dead-zone nonlinearity used in simulations is the hard-type (Fig. 2). Only one every one hundred samples is plotted in order to obtain smooth simulation curves. The signal-to-noise ratio is defined as $\mathrm{SNR} = 10\log_{10}(r_x/r_z)$.

Example 1. White input signal, $r_z = 10^{-6}$, $\mu = 0.0001$, the plant is a real acoustic response with 128 coefficients (Fig. 5), $\tau = [10^{-10}, 0.02, 0.1]$.

Example 2. Correlated input signal generated by a first-order autoregressive model given by $x(n) = a_1 x(n-1) + u(n)$, with $a_1 = 0.4$ and $r_u = E\{u^2(n)\} = 0.84$. $r_z = 10^{-6}$, $\mu = 0.0003$; $\tau = [10^{-10}, 0.02, 0.1]$. The plant impulse response is a Hanning window with unit norm ($\mathbf{w^{o\mathrm{T}}w^o} = 1$) and 30 coefficients.

Example 3. Same set of parameters as in Example 2 but with $a_1 = 0.7$, $r_u = 0.51$ and $\mu = 0.0001$.

Fig. 6 presents EMSE comparisons between analytical models and Monte Carlo simulations for Example 1. Three situations were visualized for different degrees of nonlinearity. Analytical models and simulation results are superimposed, demonstrating the good results for the white case. From these results it is clear the significant impact of the dead-zone nonlinearity on the performance of the adaptive filter, as well as the predicting capability of the developed theoretical models.

[3] $\mu_{\max}$ has been determined by simulation.

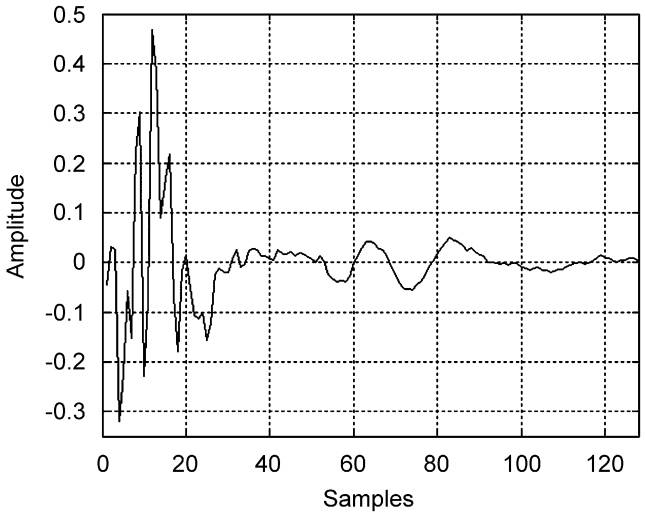

Fig. 5. Real acoustic impulse response.

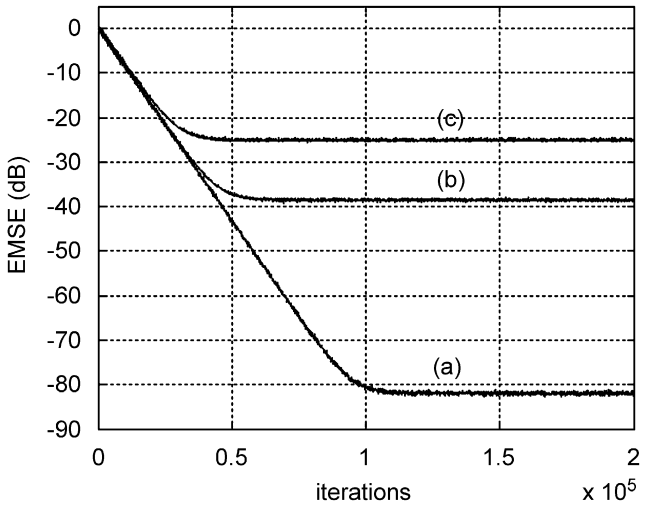

Fig. 6. Excess mean-square error (EMSE) for Example 1. White input signals with unit power, $r_z = 10^{-6}$, plant with 128 coefficients (Fig. 5). (a) Linear case ($\tau = 10^{-10}$); (b) $\eta^2 = 3927$ ($\tau = 0.02$); (c) $\eta^2 = 157$ ($\tau = 0.1$). Only one in each 100 samples is plotted in order to obtain smoother curves. Analytical and simulated results are superimposed.

Figs. 7 and 8 present results for the correlated cases. Cases (b) and (c), for both figures, present a very good match between simulations and theoretical models. Case (a) illustrates that transient theoretical predictions loose accuracy for almost linear conditions and correlated input signals. However, steady-state results are always very accurate.

Table 1 compares the simulated steady-state weight multiplicative factor ($||\lim_{n\to\infty}\mathbf{w}(n))||/||\mathbf{w^o}||$, where $||\cdot||$ is the squared norm operator) and the

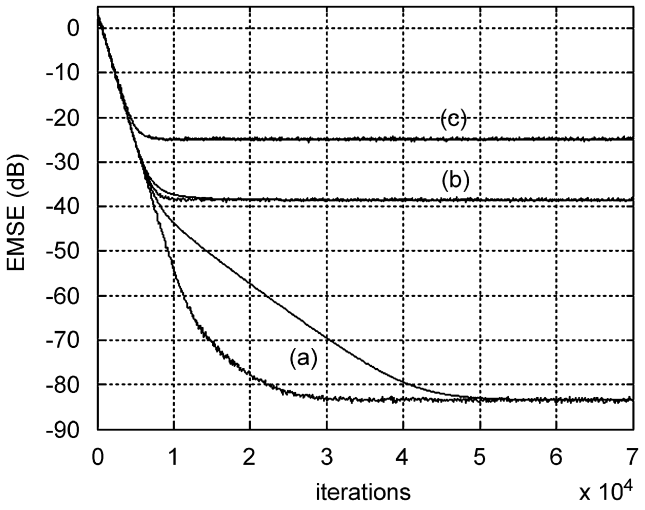

Fig. 7. Excess mean-square error (EMSE) for Example 2. Correlated input signal ($a_1 = 0.4$), $r_z = 10^{-6}$, plant obtained from a normalized Hanning window with 30 taps. (a) Linear case ($\tau = 10^{-10}$); (b) $\eta^2 = 9030$ ($\tau = 0.02$); (c) $\eta^2 = 361$ ($\tau = 0.1$). Only one in each 100 samples is plotted in order to obtain smoother curves. With exception of case (a) analytical and simulated results are superimposed.

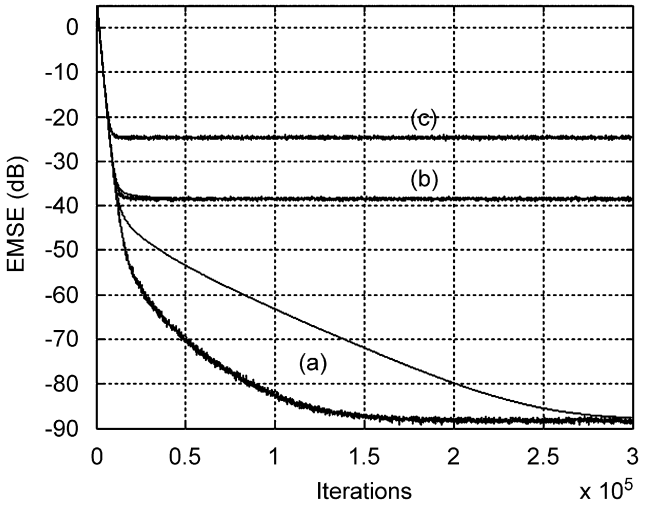

Fig. 8. Excess mean-square error (EMSE) for Example 3. Correlated input signal ($a_1 = 0.7$), $r_z = 10^{-6}$, plant obtained from a normalized Hanning window with 30 taps. (a) Linear case ($\tau = 10^{-10}$); (b) $\eta^2 = 9030$ ($\tau = 0.02$); (c) $\eta^2 = 361$ ($\tau = 0.1$). Only one in each 100 samples is plotted in order to obtain smoother curves. With exception of case (a) analytical and simulated results are superimposed.

theoretical predictions obtained from Eq. (22) for Examples 1–3. The results illustrate the accuracy of the developed analytical expression. Table 2 presents comparisons between simulated and theoretical steady-state EMSE. It is possible to verify the excellent predictions obtained using Eq. (25).

Table 1
Comparisons between simulated and predicted steady-state weight vector from Eq. (22)

τ	Example 1		Example 2		Example 3	
	Simulated	Eq. (22)	Simulated	Eq. (22)	Simulated	Eq. (22)
0.0001	1.0001	1.0001	1.0001	1.0001	1.0000	1.0000
0.001	1.0008	1.0008	1.0005	1.0005	1.0004	1.0004
0.01	1.0080	1.0080	1.0053	1.0053	1.0035	1.0035
0.1	1.0797	1.0796	1.0528	1.0526	1.0352	1.0350

Values expressed as $||\lim_{n\to\infty}\mathbf{w}(n)||/||\mathbf{w}^{\mathbf{o}}||$.

Table 2
Comparisons between simulated steady-state excess mean-square error and theoretical results obtained from Eq. (25)

τ	Example 1		Example 2		Example 3	
	Simulated	Eq. (25)	Simulated	Eq. (25)	Simulated	Eq. (25)
0.0001	−80	−84.4	−80.9	−84.4	−82.9	−84.4
0.001	−64.3	−64.4	−64.3	−64.4	−64.4	−64.4
0.01	−44.4	−44.5	−44.4	−44.5	−44.4	−44.4
0.1	−25	−25.2	−24.8	−24.9	−24.7	−24.8

Values expressed in dB.

However, since the influence of the second-order moments was neglected, the prediction error increases as the system tends to the linear case.

8. Experimental results

This section presents real laboratory experiments to verify the accuracy of the analytical models.

The LMS adaptive algorithm was implemented in a digital signal processor board (Analog Devices ADSP 21061 processor, Ez-Kit Lite evaluation platform) with some modifications (explained later) in order to compensate for filtering operations (due to the intrinsic analog filters needed for the correct signal acquisition procedure). In order to provide a controllable dead-zone nonlinearity at the output of the adaptive filter, a real class B power amplifier was placed between the digital-to-analog (DA) converter output and the analog-to-digital (AD) converter input of the DSP platform. The implemented system is shown in Fig. 9 and the power amplifier circuitry is shown in Fig. 10. A host personal computer was used for visualization of the results. Reconstruction and anti-aliasing filters that incorporate

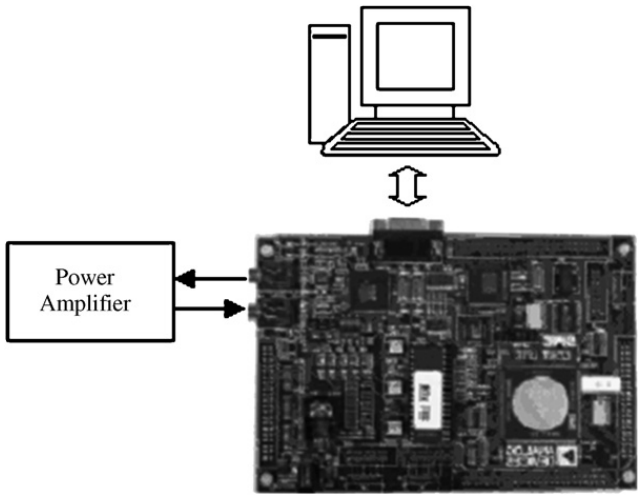

Fig. 9. Practical experiment. A class B power amplifier is placed at the output of the adaptive filter. Results are transferred to a host personal computer.

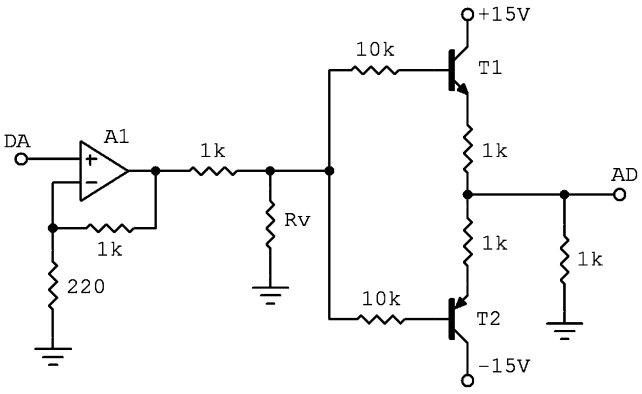

Fig. 10. Class B power amplifier used in the practical experiment. DA and AD are respectively the output and input of the digital-to-analog and analog-to-digital converters.

the CODEC (responsible for AD and DA conversion) generate filtering processes in the secondary-path (represented by block **S** in Fig. 11a) in a way that the basic setup of Fig. 1 cannot be effectively obtained. Fig. 11a presents the detailed block diagram of the system implemented to circumvent this problem. The linear part of the secondary-path (**S**—due to the filtering processes of the CODEC) was estimated *a priori* (through off-line processing) and its estimate ($\hat{\mathbf{S}}$) was used for filtering the input signal to the plant and to the LMS update equation. Following the results presented in Ref. [25], Fig. 11b is equivalent to the block diagram of Fig. 11a under slow adaptation conditions. As a result, laboratory experiments obtained from the implementation of the block diagram of Fig. 11a were compared to analytical results corresponding to Fig. 11b. The

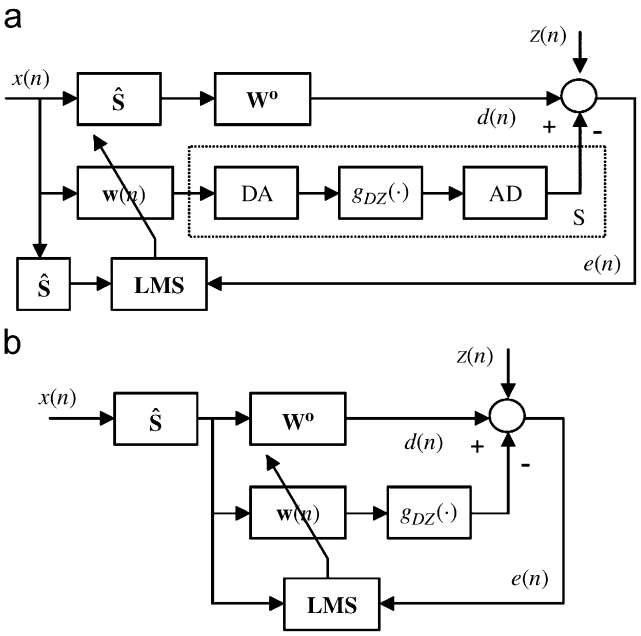

Fig. 11. Implemented block diagram (a) and equivalent one (b) [25].

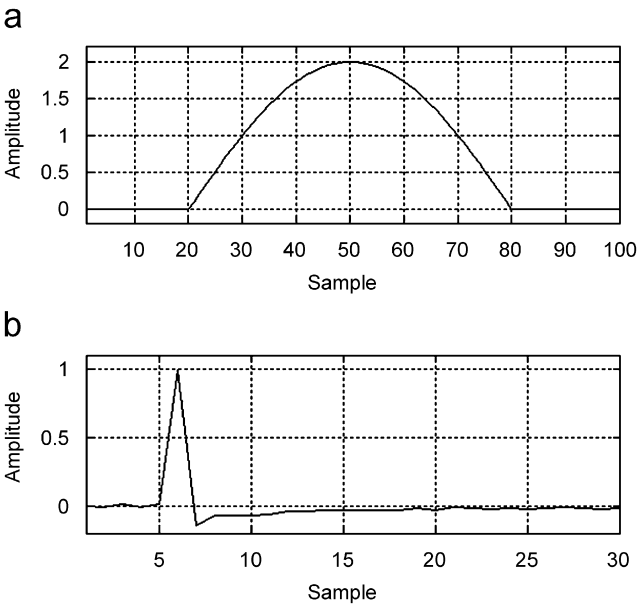

Fig. 12. Primary (a) and secondary-path (b) used in the practical experiment.

simulated plant $\mathbf{w}^{o}$ was a sampled cosine wave (Fig. 12a) and the estimated linear part of the secondary-path is shown in Fig. 12b. The experimental step size was $\mu = 0.005$ and the input signal $x(n)$ was Gaussian, white with unit power. Three experiments are presented with measured dead-zones of 0 V (linear, $\eta^2 \to \infty$), 0.33 V ($R_v = 3900\,\Omega$, $\eta^2 = 1.26$) and 0.6 V ($R_v = 2200\,\Omega$, $\eta^2 = 0.38$). The

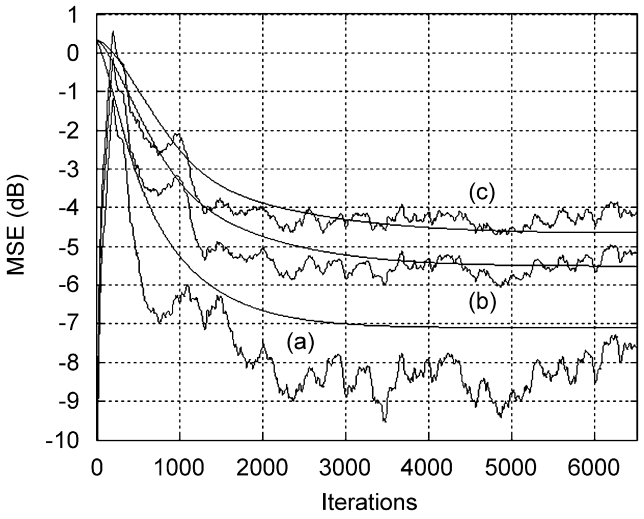

Fig. 13. Comparisons between the mean-square error (MSE) obtained from analytical and laboratory experiments. (a) Linear case ($\tau = 0\,\mathrm{V}$); (b) $\eta^2 = 1.26$ ($\tau = 0.33\,\mathrm{V}$); (c) $\eta^2 = 0.38$ ($\tau = 0.6\,\mathrm{V}$).

additive noise power was obtained from the steady-state conditions of the linear experiment (after adaptive filter convergence: $r_z = 5.39$). All experimental results were filtered by a unit norm 200-tap finite impulse response digital filter in order to smooth the obtained curves (50 runs). Finally, all curves were normalized with respect to the power level obtained without the adaptive filter (0 dB). In this example, the MSE is presented since the measurement noise sequence is unknown.

Fig. 13 presents comparisons between laboratory experiments and analytical results following the block diagrams presented in Fig. 11. It can be verified that the theoretical model is able to predict very well the impact of the dead-zone nonlinearity on the adaptive filter performance. The main sources of errors are attributed to the fact that $m \neq 1$ and to measurement errors.

9. Conclusions

This work presented a statistical analysis of the LMS algorithm behavior when subjected to a symmetric dead-zone nonlinearity at the output of the adaptive filter. This problem is of special interest in low-cost embedded multichannel ANC systems. The possibility of predictions regarding the impact of sensor or actuator nonlinearities over the performance of the LMS algorithm enables the designer to optimize the system for a tradeoff between cost and performance. Deterministic recursive equations were derived for the mean weight behavior and mean-square error for Gaussian signals and slow adaptation. Steady-state conditions were determined assuming adaptive filter convergence. Monte Carlo simulations and laboratory experiments corroborate the theoretical results.

Acknowledgments

This work was supported by the Brazilian Ministry of Science and Technology (CNPq) under grants 301866/2005-8, 307024/2006-7 and 470792/2006-0.

References

[1] M.C. Turner, Actuator deadzone compensation: theoretical verification of an intuitive control strategy, IEE Proc. Control Theory Appl. 153 (1) (January 2006) 59–68.
[2] M.L. Corradini, G. Orlando, Robust practical stabilization of nonlinear uncertain plants with input and output nonsmooth nonlinearities, IEEE Trans. Control Syst. Technol. 11 (2) (March 2003) 196–203.
[3] G. Tao, P.V. Kokotovic, Adaptive Control of Systems with Actuator and Sensor Nonlinearities, Wiley, New York, 1996.
[4] G. Tao, P.V. Kokotovic, Adaptive control of plants with unknown dead-zones, IEEE Trans. Autom. Control 39 (1) (January 1994) 59–68.
[5] A.S. Sedra, K.C. Smith, Microelectronic Circuits, Oxford, 2003.
[6] C.A. Sacher, G.F. Inbar, Tracking of the muscle recruitment characteristic during adaptive control of the electrically stimulated knee, in: Proceedings of the Annual International Conference of IEEE Engineering in Medicine and Biology Society, 1990, pp. 2315–2317.
[7] C.N. Riviere, R.S. Rader, N.V. Thakor, Adaptive canceling of physiological tremor for improved precision in microsurgery, IEEE Trans. Biomed. Eng. 45 (7) (July 1988) 839–846.
[8] M.L. Corradini, G. Orlando, Robust stabilization of nonlinear uncertain plants with backlash or dead zone in the actuator, IEEE Trans. Control Syst. Technol. 10 (1) (January 2002) 158–166.
[9] S.M. Kuo, D.R. Morgan, Active Noise Control Systems, Wiley, New York, 1996.
[10] C.R. Fuller, S.J. Elliot, P.A. Nelson, Active Control of Vibration, Academic Press, New York, 1997.
[11] P.A. Nelson, S.J. Elliot, Active Control of Sound, Academic Press, New York, 1995.
[12] N.J. Bershad, On the error saturation nonlinearities in LMS adaptation, IEEE Trans. Acoust. Speech Signal Process. 36 (4) (April 1988) 440–452.
[13] M.H. Costa, J.C.M. Bermudez, N.J. Bershad, Stochastic analysis of the filtered-X LMS algorithm in systems with nonlinear secondary paths, IEEE Trans. Signal Process. 50 (6) (June 2002) 1327–1342.
[14] M.H. Costa, J.C.M. Bermudez, N.J. Bershad, Stochastic analysis of the LMS algorithm with a saturation nonlinearity following the adaptive filter, IEEE Trans. Signal Process. 49 (7) (July 2001) 1370–1387.

[15] M.H. Costa, J.C.M. Bermudez, A new adaptive algorithm for reducing nonlinear effects from saturation in active noise control systems, Int. J. Adapt. Control Signal Process. 19 (2/3) (March/April 2005) 177–196.
[16] K.M. Tsang, G. Li, Robust nonlinear nominal-model following control to overcome deadzone nonlinearities, IEEE Trans. Ind. Electron. 48 (1) (February 2001) 177–184.
[17] T. Wigren, A. Nordsjo, Compensation of the RLS algorithm for output nonlinearities, IEEE Trans. Autom. Control 44 (October 1999) 913–1918.
[18] S. Haykin, Adaptive Filter Theory, second ed., Prentice-Hall, Englewood Cliffs, NJ, 2001.
[19] B. Widrow, S.D. Stearns, Adaptive Signal Processing, Prentice-Hall, Englewood Cliffs, NJ, 1985.
[20] D.G. Manolakis, V.K. Ingle, S.M. Kogon, Statistical and Adaptive Signal Processing: Spectral Estimation, Signal Modeling, Adaptive Filtering and Array Processing, Artech House Publishers, Boston, MA, 2005.
[21] J.E. Mazo, On the independence theory of equalizer convergence, Bell. Syst. Tech. J. 58 (May/June 1979) 963–993.
[22] A.H. Sayed, Fundamentals of Adaptive Filtering, Wiley-IEEE Press, 2003.
[23] D. Zwillinger, Standard Mathematical Tables and Formulae, CRC Press, Boca Raton, FL, 1996.
[24] A. Papoulis, S.U. Pilai, Probability, Random Variables and Stochastic Processes, fourth ed., McGraw-Hill, New York, 2002.
[25] L.S. Resende, J.C.M. Bermudez, An efficient model for convergence behavior of the FXLMS algorithm with Gaussian inputs, in: IEEE Workshop on Statistical Signal Processing, 2005, pp. 97–102.